# Tetrathiafulvalene-[2.2]paracyclophanes: Synthesis, crystal structures, and chiroptical properties

Cécile Mézière, Magali Allain, Cristina Oliveras-Gonzalez, Thomas Cauchy, Nicolas Vanthuyne, Laura G Sarbu, Lucian M Birsa, Flavia Pop, Narcis Avarvari

# Tetrathiafulvalene-[2.2]paracyclophanes: Synthesis, crystal structures, and chiroptical properties

Cécile Mézière[1] | Magali Allain[1] | Cristina Oliveras-Gonzalez[1] | Thomas Cauchy[1] | Nicolas Vanthuyne[2] | Laura G. Sarbu[3] | Lucian M. Birsa[3] | Flavia Pop[1] | Narcis Avarvari[1]

[1] Laboratoire MOLTECH-Anjou, UMR 6200, Université d'Angers, Angers, France

[2] Aix Marseille Univ, CNRS, Centrale Marseille, iSm2, Marseille, France

[3] Department of Chemistry, "Al. I. Cuza" University of Iasi, Iasi, Romania

**Correspondence** Narcis Avarvari and Flavia Pop, Laboratoire MOLTECH-Anjou, UMR 6200, Université d'Angers, CNRS, UFR Sciences, Bât. K, 2 Bd Lavoisier, 49045 Angers, France.
Email: narcis.avarvari@univ-angers.fr; flavia.pop@univ-angers.fr

**Funding information**
University of Angers and the CNRS; Région Pays de la Loire through the RFI LUMOMAT project; National Agency for Research

**Abstract**

Two racemic tetrathiafulvalene-[2.2]paracyclophane electron donors EDT-TTF-[2.2]paracyclophane **1** and $(COOMe)_2$-TTF-[2.2]paracyclophane **2** have been synthesized via the phosphite mediated cross coupling strategy. Chiral HPLC allowed the optical resolution of the ($R_P$) and ($S_P$) enantiomers for both compounds. Solid-state structures of ($R_P$)-**1** and (*rac*)-**2** have been determined by single crystal X-ray analysis. Intermolecular π-π and S•••S interactions are disclosed in the packing. Single crystal X-ray analysis of ($R_P$)-**1** combined with experimental and theoretical circular dichroism spectra allowed the assignment of the absolute configuration of the enantiomers of **1** and **2**.

**KEYWORDS**

[2.2]paracyclophane, chiral donors, circular dichroism, crystalline structures, enantiomer resolution, tetrathiafulvalene

## 1 | INTRODUCTION

Paracyclophanes[1-3] constitute, together with metallocenes,[4,5] platforms of choice to introduce chiral planarity in a chemical system (eq. monosubstituted [2.2]paracyclophane in Scheme 1). One of their advantages is the generally straightforward optical resolution of racemic cyclophanes by chiral HPLC, thus allowing the investigation of their chiroptical properties.[6,7] Besides the applications of [2.2]paracyclophane derivatives in enantioselective catalysis,[8] appropriate functionalization with conjugated chromophores, combined with strong through-space interaction within the [2.2]paracyclophane core,[9,10] may result in strong photoluminescence and intense circularly polarized luminescence activity.[11]

Alternatively, planar rigid photoactive and electroactive units such as aromatic bis (imides)[12] and anthraquinones[13] have been used to replace the phenyl rings in cyclophane-type structures. A particularly useful electroactive unit to be introduced into chiral systems is tetrathiafulvalene (TTF),[14] as it has previously provided chiral conductors in which differences of conductivity have been observed between the enantiopure and racemic forms due either to structural disorder[15-17] or different packings.[18,19] Moreover, synergy between conductivity and chirality through the electrical magneto-chiral anisotropy effect, providing different values of conductivity for the two enantiomeric forms when measured in a parallel magnetic field, has been observed for metallic mixed valence salts based on the dimethyl-ethylenedithio-tetrathiafulvalene (DM-EDT-TTF) donor.[20] While strategies based on stereogenic centers,[21-26] axial chirality,[27-30] helical

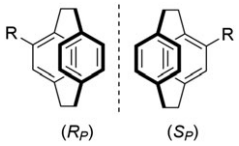


**SCHEME 1** The 2 enantiomers of monosubstituted [2.2] paracyclophane

chirality,[31] and supramolecular chirality[32,33] have been investigated in recent years, the use of [2.2]paracyclophanes as source of planar chirality to prepare enantiopure TTFs has only been reported once to the best of our knowledge.[34] In that work, modulation of the circular dichroism (CD) spectra with the oxidation state of TTF for a bis (TTF) pseudo-*ortho*-[2.2]paracyclophane has been demonstrated. Meanwhile, the synthesis of a diastereomeric mixture of a TTF-bis (paracyclophane) has been previously reported by some of us.[35] However, no solid-state structures of TTF-[2.2]paracyclophanes, enantiopure or racemic, have been reported to date.

In this work, we describe the synthesis, optical resolution, and single crystal X-ray structure of two TTF-[2.2] paracyclophane derivatives, together with their chiroptical properties supported by density functional theory (DFT) and time-dependent (TD)-DFT calculations.

## 2 | MATERIALS AND METHODS

Nuclear magnetic resonance spectra were recorded on a Bruker Avance DRX 300 spectrometer operating at 300 MHz for $^{1}H$ and 75 MHz for $^{13}C$. Chemical shifts are expressed in parts per million (ppm) downfield from external tetramethylsilane (TMS). The following abbreviations are used: s, singlet; dd, doublet of doublets; m, multiplet. MALDI–TOF MS spectra were recorded on Bruker Biflex-IIITM apparatus, equipped with a 337-nm $N_2$ laser.

### 2.1 | Syntheses

#### 2.1.1 | 6-([2.2]Paracyclophan-4-yl)-2,3-ethylenedithio-tetrathiafulavalene (*rac*)-1

4-([2.2]Paracyclophan-4-yl)-1,3-dithiol-2-thione[35] (*rac*)-**3** (414 mg, 1.20 mmol) and 4,5-ethylenedithio-1,3-dithiole-2-one **4** (476 mg, 2.40 mmol) were mixed under argon in 13 mL of freshly distilled trimethylphosphite under nitrogen. The temperature was gradually risen to 80°C, stirred for 30 minutes followed by 5 hours at 100–110°C. After cooling to room temperature, the solution was filtered to remove some of the BEDT-TTF side product. The solvent was then evaporated under reduced pressure and the oily brown residue chromatographed on silica gel using petroleum spirit/dichloromethane 1/1 to afford a brown solid (140 mg, 23%), M.p. = 110 to 112°C. Single crystals were obtained by slow evaporation of an acetonitrile solution; $^{1}H$ NMR (300 MHz, $CDCl_3$) δ 6.73 (dd, $J$ = 7.9, 1.6 Hz, 1H), 6.57 (m, 2H), 6.53–6.46 (m, 3H), 6.44 (dd, $J$ = 7.9, 1.6 Hz, 1H), 6.20 (s, 1H), 3.66-3.57 (m, 1H), 3.35-3.28 (m, 4H), 3.14-2.92 (m, 7H); $^{13}C$ NMR (75 MHz, $CDCl_3$) δ 140.26, 139.46, 139.33, 138.07, 135.97, 133.63, 133.03, 132.76, 132.64, 132.57, 132.23, 130.79, 118.85, 115.00, 114.11, 114.04, 104.17, 35.33, 35.02, 34.98, 34.38; MS (MALDI-TOF) *m/z*: 499.9 ($M_{th}$ = 499.99).

#### 2.1.2 | 6-([2.2]Paracyclophan-4-yl)-2,3-dimethoxycarbonyl-tetrathiafulavalene (*rac*)-2

4-([2.2]Paracyclophan-4-yl)-1,3-dithiol-2-thione[35] (*rac*)-**3** (450 mg, 1.32 mmol) and 4,5-dimethoxycarbonyl-1,3-dithiole-2-one **5** (309 mg, 1.32 mmol) were mixed under argon in 14 mL of freshly distilled trimethylphosphite under nitrogen. The temperature was gradually risen to 80°C, stirred for 30 minutes followed by 5 hours at 100–110°C. The solvent was evaporated under reduced pressure and the oily violet residue chromatographed on silica gel using petroleum spirit/dichloromethane 1/1 to afford a brown solid (162 mg, 31%), M.p. = 187°C. Single crystals were obtained by slow evaporation of an acetonitrile solution; $^{1}H$ NMR (300 MHz, $CDCl_3$) δ 6.72 (dd, $J$ = 7.9, 1.6 Hz, 1H), 6.58 (m, 2H), 6.49 (m, 3 Hz, 3H), 6.43 (dd, $J$ = 7.9, 1.6 Hz, 1H), 6.21 (s, 2H), 3.86 (s, 6H), 3.65-3.55 (m, 1H), 3.16-2.87 (m, 7H); $^{13}C$ NMR (75 MHz, $CDCl_3$) δ 160.10, 160.06, 140.30, 139.41, 139.33, 138.08, 136.18, 136.00, 133.75, 133.05, 132.64, 132.59, 132.49, 132.26, 132.21, 132.17, 130.69, 116.93, 114.93, 103.31, 53.34, 35.31, 35.01, 34.96, 34.35; MS (MALDI-TOF) *m/z*: 525.9 ($M_{th}$ = 526.04).

### 2.2 | Enantiomer resolution

Resolution of racemic mixtures of (*rac*)-**1** and (*rac*)-**2** was done by chiral chromatography on Chiralpak IE (250 × 10 mm), hexane/ethanol/dichloromethane (5/3/2) as mobile phase, flow-rate = 5 mL/min, UV detection at 254 nm.

(*rac*)-**1** was separated as follows: first fraction, 23 mg ((−, CD 254 nm)-enantiomer) with ee > 98.5%; and second fraction, 20 mg ((+, CD 254 nm)-enantiomer) with ee > 99%.

(*rac*)-**2** was separated as follows: first fraction, 35 mg ((−, CD 254 nm)-enantiomer) with ee > 99%; and second fraction, 35 mg ((+, CD 254 nm)-enantiomer) with ee > 99%.

### 2.3 | CD and UV measurements

Circular dichroism spectra were recorded using spectrometric grade dichloromethane in a 0.2 cm cell at sample concentrations of $5 \times 10^{-5}$ for compound **1** and $10^{-5}$ M for compound **2** for using a Jasco J-815 Circular Dichroism

Spectrometer (Biosit facility–Université de Rennes 1). Absorption spectra of compounds **1** and **2** have been recorded in spectrometric grade dichloromethane solutions of $5 \times 10^{-5}$ M and $2.5 \times 10^{-5}$ M concentrations, respectively, using a 1 cm cell.

## 2.4 | Single crystal X-ray diffraction

X-ray single-crystal diffraction data were collected on an Agilent SuperNova diffractometer equipped with Atlas CCD detector and mirror monochromated microfocus Cu-$K_\alpha$ radiation ($\lambda$ = 1.54184 Å). The structures were solved by direct methods, expanded, and refined on $F^2$ by full matrix least-squares techniques using SHELX programs (G. M. Sheldrick, 2016). All non-H atoms were refined anisotropically and the H atoms were included in the calculation without refinement. Multiscan empirical absorption was corrected using CrysAlisPro program (CrysAlisPro, Agilent Technologies, V1.171.37.35 g, 2014). A summary of the crystallographic data and the structure refinement is given in Table 1. CCDC 1811254 ($R_P$)-**1** and CCDC 1811262 (*rac*)-**2** contain the supplementary crystallographic data for this paper. These data can be obtained free of charge from The Cambridge Crystallographic Data Centre via www.ccdc.cam.ac.uk/data_request/cif.

## 2.5 | Electrochemical studies

Cyclic voltammetry measurements were performed with a Biologic SP-150 potentiostat under argon, by using a 3-electrode cell equipped with a platinum millielectrode of 0.126 $cm^2$ area, an $Ag/Ag^+$ pseudoreference electrode, and a platinum wire counter electrode. The potential values are reported with respect to ferrocene (oxidation potential of ferrocene is fixed at zero). The electrolytic media involved a 0.1 mol/L solution of ($n$-$Bu_4N$)$PF_6$ in acetonitrile. All experiments were performed at room temperature at 0.1 V/s.

**TABLE 1** Crystallographic data, details of data collection, and structure refinement parameters

| | (***R*****$_P$**)-1 | (***rac***)-2 |
|---|---|---|
| Formula | $C_{24}H_{20}S_6$ | $C_{26}H_{22}O_4S_4$ |
| $M$, $gmol^{-1}$ | 500.76 | 526.68 |
| $T$, K | 200.0(1) K | 180.0(1) K |
| Crystal system | Monoclinic | Monoclinic |
| Space group | $P2_1$ | $P2_1/c$ |
| $a$, Å | 7.4706(2) | 27.777(1) |
| $b$, Å | 11.7648(3) | 11.3146(6) |
| $c$, Å | 13.0617(4) | 7.6036(5) |
| $\beta$, ° | 100.454(3) | 96.992(6) |
| $V$, $Å^3$ | 1128.94(5) | 2371.9(2) |
| $Z$ | 2 | 4 |
| $\rho_{calcd}$, $gcm^{-3}$ | 1.473 | 1.475 |
| $\mu$, $mm^{-1}$ | 5.667 | 3.954 |
| Goodness-of-fit on $F^2$ | 1.041 | 1.118 |
| Final R1/$w$R2 [$I > 2\sigma$(I)] | 0.0480/0.1218 | 0.0696/0.2047 |
| R1/$w$R2 (all data) | 0.0524/0.1265 | 0.0758/0.2154 |
| Absolute structure parameter | 0.01(3) | |

## 2.6 | Density functional theory calculations

All calculations have been performed with the Gaussian09 program[36] using the DFT method with the hybrid PBE0 functional (with 25% of exact exchange)[37,38] and the augmented and polarized Pople-type basis set 6–311++G(2df,pd). An ultrafine integration grid was chosen. First, the gas-phase ground-state geometries were optimized, starting from the X-Ray diffraction data. The gas-phase excited-states energies were then determined by a linear response TD-DFT method. The length gauge formulation was used for the calculation of the rotatory strengths, but both formulas give practically the same values. The calculated spectra have been enlarged by a Gaussian shape (full width at half-maximum [FWHM] = 3000 $cm^{-1}$ for UV-visible and 0.3 eV for CD plots) with GaussSum to compare with the experimental data.[39] The computational results reports, molecular orbitals, and density difference plots were prepared with ABSiCC, a homemade program.[40]

# 3 | RESULTS AND DISCUSSION

The syntheses of paracyclophane-TTFs (*rac*)-**1** and (*rac*)-**2** have been done by phosphite mediated heterocoupling between the 4-([2.2]paracyclophan-4-yl)-1,3-dithiol-2-thione (*rac*)-**3** previously described[35] and the corresponding 1,3-dithiole-2-ones (**4** and **5**) (Scheme 2). Both (*rac*)-**1** and (*rac*)-**2** have been separated by chiral chromatography in the corresponding enantiomers ($S_p$)/($R_p$) with enantiomeric excesses superior to 99%.

The absolute configuration of derivatives **1** has been determined by single crystal X-ray analysis, suitable crystals of the second eluted enantiomer (+, CD) being obtained by slow evaporation of an acetonitrile solution. The (+, CD)-**1** enantiomer has crystalized in the monoclinic system, $P2_1$ polar space group, with one independent molecule in the asymmetric unit. Thus for derivatives **1**, the second eluted enantiomer (+, CD) corresponds to the ($R_P$) enantiomer (Figure 1).

The same conditions for crystal growing have been successfully applied on the racemic form of paracyclophane-TTF (*rac*)-**2**. The two symmetry-related

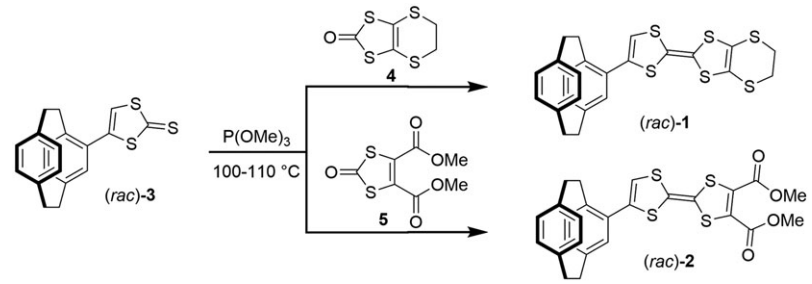


**SCHEME 2** Syntheses of racemic [2.2] paracyclophane-TTFs. Only the ($S_P$) enantiomers are represented

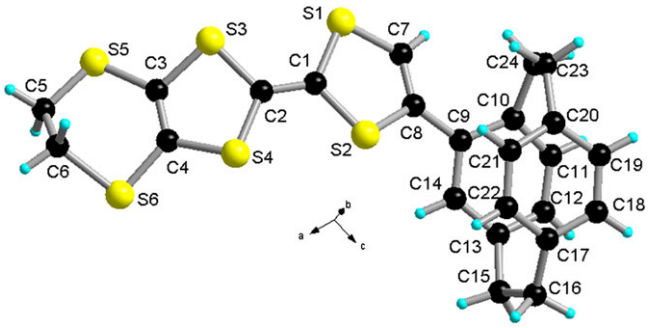

**FIGURE 1** Solid state structure of ($R_P$)-1 enantiomer with atomic labels

forms that crystalize in the monoclinic system, $P2_1/c$ space group with one independent molecule in the asymmetric unit, are displayed in Figure 2.

($R_P$)-**1** shows a classical edge-to-face herringbone packing in both the *ab* and *bc* planes with alternating stacks formed of molecules with almost orthogonal orientation, whereas the view along the *b* axis suggests segregation between the TTFs and the paracyclophanes (Figures S1 and S2). In the *ab* plane, packing between the alternating stacks is ensured by ArH•••π interactions of the paracyclophane units, whereas in the *bc* plane, lateral short S•••S distances of about 3.94 Å have been observed between the TTF units of the orthogonal molecules. Within each column, molecules stacked on top of each other are laterally and longitudinally shifted because of steric impediments of the paracyclophane units. Similarly, the large

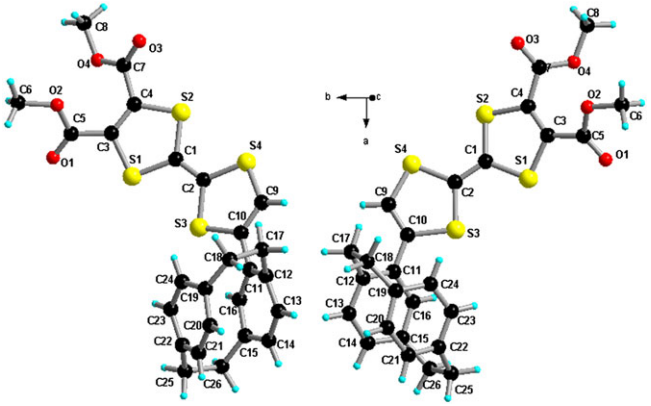

**FIGURE 2** The two enantiomers ($R_P$) (left) and ($S_P$) (right) in the solid state structure of (*rac*)-2 with atomic labels

dihedral angle between the TTF and the phenyl unit suggests steric impediments of the TTF with the proton atoms of the paracyclophane bridge. Nevertheless, S•••S distances of about 4.08 Å have been observed between the TTF units within the stack (Figure 3 and Table 2).

The packing of (*rac*)-**2** shows a clear segregation between the TTF and the paracyclophane units both in the *ab* and *ac* planes (Figure S3 and S4). In the *ab* plane, molecules alternate in an orthogonal fashion showing short interplanar distances between the TTF units of 3.67 Å of the neighboring layers (Table 2). Within each of the layers (for example, bottom layer highlighted in red), molecules pack through hydrogen bonding interactions of the ester units OMe•••O═C of 2.46 Å. Between the parallel layers, molecules pack through ArH•••π interactions of the paracyclophane units of 3.08 and 3.11 Å (Figure 4). The lack of any notable S•••S interactions and stacking of the TTFs in overlapped fashion, despite the short interplanar distance, together with the larger TTF-Ph dihedral angle, suggesting a higher distortion of the molecular geometry in (*rac*)-**2** compared to ($R_P$)-**1**, is an indicative of the less favorable packing of the racemic with respect to the enantiopure material in the neutral state. Similar packing has been observed for the starting material (*rac*)-**3** with the exception of any notable ArH•••π interactions.[35] Despite the presence of some short S•••S distances between the C═S and the $S_{dithiolene}$ of 3.76 and 3.86 Å, no π-π overlap has been observed in the structure of (*rac*)-**3**; therefore, molecules seem to be less compact and shifted because of lack of any notable interactions driving the packing (Figure S5).

Cyclic voltammetry measurements of **1** and **2**, performed in dichloromethane electrolyte solution, show the expected pair of one electron reversible oxidation processes corresponding to the formation of the radical cation and the dication at 0.02 and 0.47 V and 0.14 and 0.62 V versus $Fc/Fc^+$, respectively (Table 3). The values of the redox potentials are anodically shifted relative to TTF 4,12-disubtituted-[2.2]paracyclophane[34] where formation of mixed valence state has been observed because of the presence of two TTF units within the same molecule. Nevertheless, the observed values are similar to phenyl-di(thiomethyl)-TTF and di(thiomethyl)-TTF

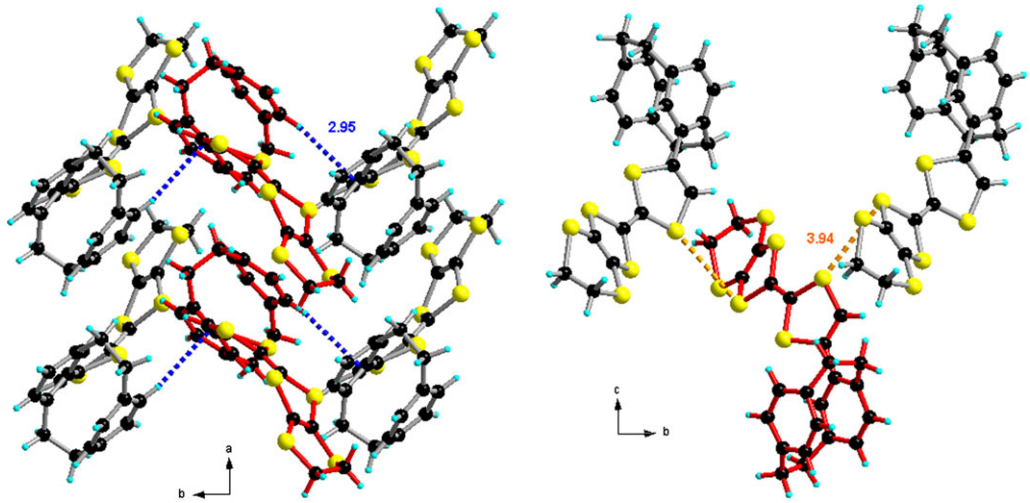


**FIGURE 3** Packing of ($R_P$)-1 in the ab (left) and bc (right) planes (alternating stacks highlighted in red for clarity)

**TABLE 2** Values of the S•••S distances, ArH•••π (centroid of phenyl unit of the paracyclophane), inter-TTF planes distances (Å) together with dihedral angles (°) between the planes of TTF and the adjacent phenyl ring of the paracyclophane (TTF-Ph) for compounds ($R_P$)-**1** and (*rac*)-**2**

| Compound | S•••S, Å Intrastack | S•••S, Å Interstack | ArH•••π, Å | Inter-TTF Plane Distance, Å | TTF-Ph, ° |
|---|---|---|---|---|---|
| ($R_P$)-**1** | 4.08 | 3.94 | 2.95 | 4.64 | 27.36 |
| (*rac*)-**2** | | | 3.08 3.11 | 3.67 | 44.31 |

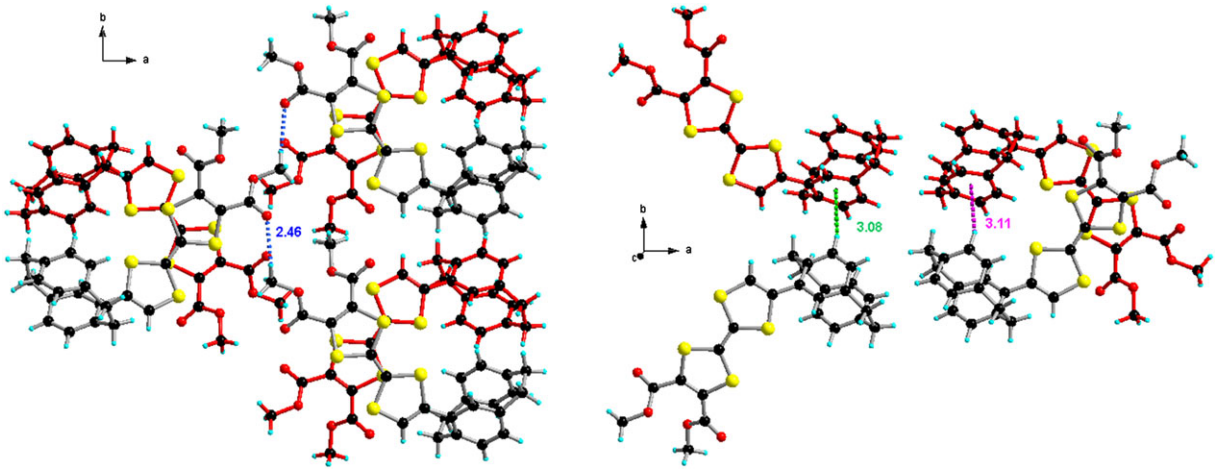


**FIGURE 4** Packing of (*rac*)-2 in the ab plane (orthogonal parallel layers highlighted in red), together with OMe•••O=C interactions of the top layer (left) and ArH•••π interaction between layers (right)

**TABLE 3** Half-wave potentials relative to $Fc/Fc^+$ of compounds **1** and **2**[a]

| Compound | $E^1_{ox}$ | $E^2_{ox}$ |
|---|---|---|
| **1** | 0.02 | 0.47 |
| **2** | 0.14 | 0.62 |
| TTF-$(SMe)_2$[27] | 0.03 | 0.35 |
| Ph-TTF-$(SMe)_2$[34] | 0.00 | 0.37 |

[a]Cyclic voltammograms were recorded in dichloromethane $10^{-1}$ M $TBAFP_6$ electrolyte solutions at 20°C, and potentials reported as $E_{1/2}$ (= $(E_p^a + E_p^c)/2$) in V versus $Fc/Fc^+$ at 0.1 $Vs^{-1}$ scan rate (experimental value of $Fc/Fc^+$ adjusted to 0).

suggesting no significant influence of the paracyclophane unit on the oxidation potentials (Table 3). Both the first and second oxidation values are lower in **1** compared to **2** in which the electron withdrawing effect of the two carbonyl units reduces its donor ability. This electron withdrawing effect appears clearly on the energy and topology of the calculated frontier molecular orbitals (Tables 4 and 5). In both cases, the HOMO corresponds to the TTF moiety, and it has higher stability, by 0.2 eV for compound **2**, as expected from the oxidation potentials. The LUMO orbital is however different since it is localized on the paracyclophane unit for compound **1** and on the ester part

**TABLE 4** Frontier molecular orbitals plots and energies of compound **1**

| MO | Energy | Plot |
|---|---|---|
| LUMO | −1.42 | 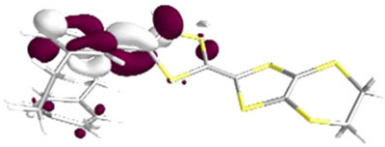 |
| HOMO | −4.94 | 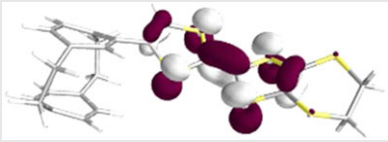 |

**TABLE 5** Frontier molecular orbitals plots and energies of compound **2**

| MO | Energy | Plot |
|---|---|---|
| LUMO | −1.97 | 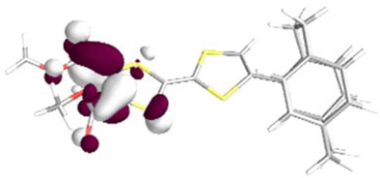 |
| HOMO | −5.11 | 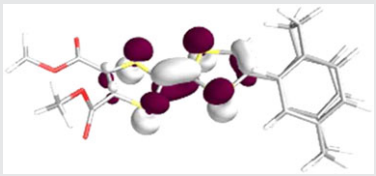 |

of compound **2**, thus being much lower in energy for the latter than for the former.

The resolved enantiomers of both **1** and **2** have been studied by CD. The mirror-image spectra of both pairs of enantiomers in dichloromethane solutions are displayed in Figures 5 and 6. Both derivatives show a first intense band peaking at 296 nm, two medium bands at 325 and 350 nm, followed by one large band of weak intensity for enantiomers of **2**, and two bands of low intensity at 395 and 435 nm in the case of enantiomers of **1** (Figure 6). By analogy to compounds **1** solid structure absolute configuration and the CD detection at 254 nm during the enantiomer resolution, together with the comparison with the previously described bis(TTF)-paracyclophane compound,[34] the positive CD signal at 296 nm has been attributed to conformer ($R_P$)-**2** while the negative one has been attributed to conformer ($S_P$)-**2**.

The theoretical CD spectrum of ($R_P$)-**1** (CD (+)-**1**) accurately reproduces the experimental results with the exception of a small blue shift off all bands. The band at 435 nm is predicted at about 428 nm with higher intensity, being

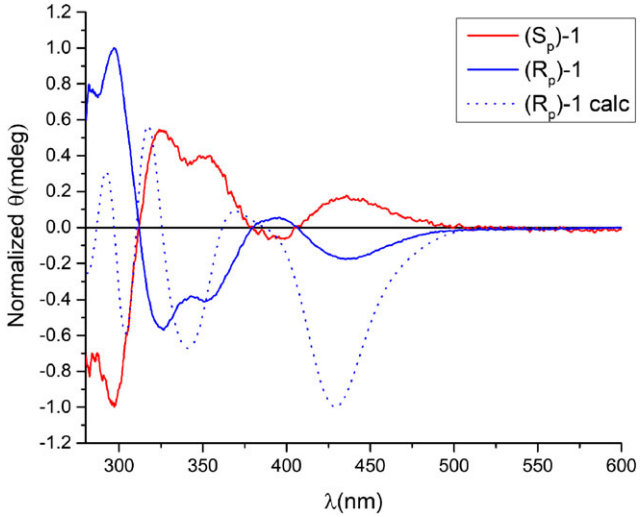


**FIGURE 5** CD spectra of ($S_P$)-1 (CD (−)-1 red line) and ($R_P$)-1 (CD (+)-1 blue line) together with the calculated for ($R_P$)-1 (CD (+)-1 blue dotted line)

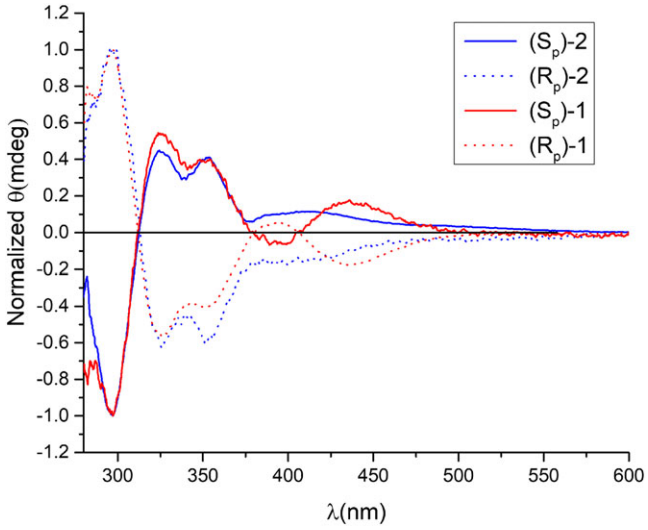


**FIGURE 6** CD spectra of ($S_P$)-1 (CD (−)-1 red line) and ($R_P$)-1 (CD (+)-1 red dotted line) together with the 2 forms of derivative 2 (blue line for ($S_P$)-2 (CD (−)-2 and blue dotted line for ($R_P$)-2 (CD (+)-2))

assigned to the $S_0$ to $S_2$ excitation, while the following positive band is attributed to an $S_0$ to $S_3$ excitation, and the first of the two medium negative bands corresponds to the $S_0$ to $S_4$ excitation. The first intense band at 296 nm was not included in the calculation (Figure 5 and Table 6).

For compound **2**, the TD-DFT calculation has been run on the ($R_P$) enantiomer, and the results were unsatisfactory because the gas phase converged geometry kept one of the ester group heavily distorted from the TTF median plan by 59.4°. Therefore, any excitation including a TTF to ester excitation (HOMO to LUMO) will generate an artificial electronic rotation, namely, a CD signal, whereas in solution at room temperature, the free rotation

**TABLE 6** Excited singlet states calculated wavelengths, oscillator and rotatory strengths, and electron density difference plots (where a blue surfaces indicate the excited electron density and the white surfaces indicate the hole) for compound **1**

| Excitation | $\lambda_{max,\ calc}$, nm | $\lambda_{max,\ exp}$, nm | Oscillator Strength | Rotatory Strength | EDD Plot |
|---|---|---|---|---|---|
| $S_0 \rightarrow S_2$ | 428 | 435 | 0.06 | −62 | 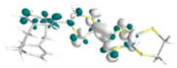 |
| $S_0 \rightarrow S_3$ | 369 | 395 | 0.01 | 27 | 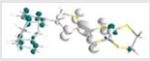 |
| $S_0 \rightarrow S_4$ | 340 | 350 | 0.03 | −44 | 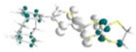 |

of the ester groups will minimize this impact on the CD spectra (Figures S6 and S7).

## 4 | CONCLUSION

This work describes the straightforward synthesis of EDT-TTF-[2.2]paracyclophane **1** and $(COOMe)_2$-TTF-[2.2] paracyclophane **2** donors as racemic mixtures with the objective to take advantage of the planar chirality of the rigid cyclophane unit. The chiral resolution of the ($R_P$) and ($S_P$) enantiomers has been performed by chiral HPLC, whereas the single crystal X-ray structure of ($R_P$)-**1** in combination with CD measurements supported by TD-DFT calculations allowed the assignment of the absolute configurations. Besides the classical intermolecular interactions in the packing of TTF-based materials through S•••S contacts, notable ArH•••π interactions of the paracyclophane units have been observed to reinforce the packing of both compounds. The DFT calculations emphasized the important role of the TTF substituents on the molecular orbitals, especially the LUMO, as in compound **1**, the LUMO is based on the cyclophane unit, while in **2**, it is spread over the ester substituents. The facile synthesis and optical resolution of TTF-[2.2] paracyclophanes described herein open the way towards the preparation of planar chiral radical cation salts, while the solid-state packing shows encouraging potential for their use in chiral bulk materials with interesting conducting properties.


### ACKNOWLEDGMENTS

Financial support from the National Agency for Research (ANR, Project Chirafun 09-BLAN-0045-01), the Région Pays de la Loire through the RFI LUMOMAT project (grant to C. O.-G.), and the University of Angers and the CNRS are gratefully acknowledged. Biosit facility (Université de Rennes 1) is acknowledged for the access to the CD instrument.



1. Vögtle F. *Cyclophane Chemistry: Synthesis.* Chichester: Structures and Reactions. Ed. John Wiley & Sons; 1993.
2. Gleiter R, Hopf HMC. In: Weinheim, ed. *Chemistry.* Wiley-VCH; 2004.
3. Aly AA, Brown AB. Asymmetric and fused heterocycles based on [2.2]paracyclophane. *Tetrahedron*. 2009;65:8055-8089.
4. Schaarschmidt D, Lang H. Selective syntheses of planar-chiral ferrocenes. *Organometallics*. 2013;32:5668-5704.
5. Gao D-W, Gu Q, Zheng C, You S-L. Synthesis of planar chiral ferrocenes via transition-metal-catalyzed direct C−H bond functionalization. *Acc Chem Res*. 2017;50:351-365.
6. Mori T, Inoue Y. Recent theoretical and experimental advances in the electronic circular dichroisms of planar chiral cyclophanes. *Top Curr Chem*. 2011;298:99-128.
7. Grimme S, Harren J, Sobanski A, Vögtle F. Structure/chiroptics relationships of planar chiral and helical molecules. *Eur J Org Chem*. 1998;1491-1509.
8. Pye PJ, Rossen K, Reamer RA, Tsou NN, Volante RP, Reider PJ. A new planar chiral bisphosphine ligand for asymmetric catalysis: highly enantioselective hydrogenations under mild conditions. *J Am Chem Soc*. 1997;119:6207-6208.
9. Bartholomew GP, Bazan GC. Bichromophoric paracyclophanes: models for interchromophore delocalization. *Acc Chem Res*. 2001;34:30-39.
10. Bazan GC. Novel organic materials through control of multichromophore interactions. *J Org Chem*. 2007;72:8615-8635.
11. Morisaki Y, Gon M, Sasamori T, Tokitoh N, Chujo Y. Planar chiral tetrasubstituted [2.2]paracyclophane: optical resolution and functionalization. *J Am Chem Soc*. 2014;136:3350-3353.
12. Spenst P, Würthner F. Photo- and redoxfunctional cyclophanes, macrocycles, and catenanes based on aromatic bisimides. *J Photochem Photobiol C: Photochem Rev*. 2017; 31:114–138.

13. Farrán A, Mohanraj J, Clarkson GJ, Claramunt RM, Herranz F, Accorsi G. Tuning photoinduced processes of covalently bound isoalloxazine and anthraquinone bichromophores. *Photochem Photobiol Sci*. 2013;12:813–822.

14. Avarvari N, Wallis JD. Strategies towards chiral molecular conductors. *J Mater Chem*. 2009;19:4061–4076.

15. Réthoré C, Avarvari N, Canadell E, Auban-Senzier P, Fourmigué M. Chiral molecular metals: syntheses, structures and properties of the AsF6− salts of racemic (+/−), (R)- and (S)-tetrathiafulvalene-oxazoline derivatives. *J Am Chem Soc*. 2005;127:5748-5749.

16. Madalan AM, Réthoré C, Fourmigué M, et al. Order versus disorder in chiral tetrathiafulvalene–oxazolines radical cation salts: structural, theoretical investigations and physical properties. *Chem A Eur J*. 2010;16:528-537.

17. Pop F, Laroussi S, Cauchy T, Gómez-García CJ, Wallis JD, Avarvari N. Tetramethyl bis (ethylenedithio)-tetrathiafulvalene (TM-BEDT-TTF) revisited: crystal structures, chiroptical properties, theoretical calculations and a complete series of conducting radical cation salts. *Chirality*. 2013;25:466-474.

18. Pop F, Auban-Senzier P, Frąckowiak A, et al. Chirality driven metallic versus semiconducting behavior in a complete series of radical cation salts based on dimethyl-ethylenedithio-tetrathiafulvalene (DM-EDT-TTF). *J Am Chem Soc*. 2013;135:17176-17186.

19. Pop F, Auban-Senzier P, Canadell E, Avarvari N. Anion size control of the packing in the metallic versus semiconducting chiral radical cation salts (DM-EDT-TTF)2XF6 (X = P, as, Sb). *Chem Commun*. 2016;52:12438-12441.

20. Pop F, Auban-Senzier P, Canadell E, Rikken GLJA, Avarvari N. Electrical magneto-chiral anisotropy in a bulk chiral molecular conductor. *Nat Commun*. 2014;5:3757.

21. Réthoré C, Fourmigué M, Avarvari N. Tetrathiafulvalene based phosphino-oxazolines: a new family of redox active chiral ligands. *Chem Commun*. 2004;1384-1385.

22. Réthoré C, Fourmigué M, Chiral AN. Tetrathiafulvalene–hydroxyamides and –oxazolines: hydrogen bonding, chirality, and a radical cation salt. *Tetrahedron*. 2005;61:10935-10942.

23. Griffiths J-P, Nie H, Brown RJ, Day P, Wallis JD. Synthetic strategies to chiral organosulfur donors related to bis (ethylenedithio) tetrathiafulvalene. *Org Biomol Chem*. 2005;3:2155-2166.

24. Riobé F, Avarvari N. $C_2$-symmetric chiral tetrathiafulvalene-bis (oxazolines) (TTF-BOX): new precursors for organic materials and electroactive metal complexes. *Chem Commun*. 2009;3753-3755.

25. Yang S, Brooks AC, Martin L, et al. Novel enantiopure bis (pyrrolo) tetrathiafulvalene donors exhibiting chiral crystal packing arrangements. *Cryst Eng Comm*. 2009;11:993-996.

26. Chas M, Lemarié M, Gulea M, Avarvari N. Chemo- and enantioselective sulfoxidation of bis (ethylenedithio)-tetrathiafulvalene (BEDT-TTF) into chiral BEDT-TTF-sulfoxide. *Chem Commun*. 2008;220-222.

27. Hasegawa M, Sone Y, Iwata S, Matsuzawa H, Mazaki Y. Tetrathiafulvalenylallene: a new class of donor molecules having strong chiroptical properties in neutral and doped states. *Org Lett*. 2011;13:4688-4691.

28. Gómez R, Segura JL, Martin N. New chiral binaphthyl building blocks: synthesis of the first optically active tetrathiafulvalene and 11, 11, 12, 12-tetracyano-9, 10-anthraquinodimethane dimers. *J Org Chem*. 2000;65:7566-7574.

29. Zhou Y, Zhang D, Zhu L, Shuai Z, Zhu D. Binaphthalene molecules with tetrathiafulvalene units: CD Spectrum modulation and new chiral molecular switches by reversible oxidation and reduction of tetrathiafulvalene units. *J Org Chem*. 2006;71:2123-2130.

30. Saad A, Barrière F, Levillain E, Vanthuyne N, Jeannin O, Fourmigué M. Persistent mixed-valence $[(TTF)_2]^{+\bullet}$ dyad of a chiral bis (binaphthol)–tetrathiafulvalene (TTF) derivative. *Chem A Eur J*. 2010;16:8020-8028.

31. Biet T, Fihey A, Cauchy T, et al. Ethylenedithio-tetrathiafulvalene-helicenes: Electroactive helical precursors with switchable chiroptical properties. *Chem A Eur J*. 2013;19:13160-13167.

32. Danila I, Riobé F, Piron F, et al. Hierarchichal chiral expression from the nano to meso-scale in supramolecular helical fibres of a non-amphiphilic $C_3$-symmetrical $\pi$-functional molecule. *J Am Chem Soc*. 2011;133:8344-8353.

33. Pop F, Melan C, Danila I, et al. Hierarchical self-assembly of supramolecular helical fibres from amphiphilic $C_3$-symmetrical functional tris (tetrathiafulvalenes). *Chem A Eur J*. 2014;20:17443-17453.

34. Kobayakawa K, Hasegawa M, Sasaki H, et al. Dimeric tetrathiafulvalene linked to *pseudo-ortho*-[2.2]paracyclophane: chiral electrochromic properties and use as a chiral dopant. *Chem Asian J*. 2014;9:2751-2754.

35. Sarbu LG, Bahrin LG, Jones PG, Birsa LM, Hopf H. [2.2] Paracyclophane derivatives containing tetrathiafulvalene moieties. *Beilst J Org Chem*. 2015;11:1917-1921.

36. Frisch MJ, Trucks GW, Schlegel HB, et al. *Gaussian 09, rev. D.01*. Wallingford CT: Gaussian, Inc.; 2009.

37. Burke K, Ernzerhof M, Perdew JP. The adiabatic connection method: a non-empirical hybrid. *Chem Phys Lett*. 1997;265:115-120.

38. Adamo C, Barone V. Toward reliable density functional methods without adjustable parameters: the PBE0 model. *J Chem Phys*. 1999;110:6158;-6170.

39. O'boyle NM, Tenderholt AL, Langner KM. Cclib: a library for package-independent computational chemistry algorithms. *J Comput Chem*. 2008;29:839;-845.

40. ABSiCC, Automating Boring Stuff in Computational Chemistry, designed by Thomas Cauchy and maintained by Yohann Morille, Angers University.